Applied Catalysis B: Environmental 117–118 (2012) 59–66

Contents lists available at SciVerse ScienceDirect

Applied Catalysis B: Environmental

journal homepage: www.elsevier.com/locate/apcatb

Hydrothermal synthesis of $BiVO_4$: Structural and morphological influence on the photocatalytic activity

S. Obregón, A. Caballero, G. Colón*

Instituto de Ciencia de Materiales de Sevilla, Centro Mixto Universidad de Sevilla-CSIC, C/Américo Vespucio, 49, 41092 Sevilla, Spain

ARTICLE INFO

Article history:
Received 14 November 2011
Received in revised form
13 December 2011
Accepted 22 December 2011
Available online 31 December 2011

Keywords:
Hydrothermal
$BiVO_4$
Photocatalysis
Methylene blue

ABSTRACT

$BiVO_4$ hierarchical heterostructures are synthesized by means of a surfactant free hydrothermal method having good photoactivities for the degradation of methylene blue under UV–vis irradiation. From the structural and morphological characterization it has been stated that $BiVO_4$ present the monoclinic crystalline phase with different morphologies depending on the pH value, type of precipitating agent and hydrothermal temperature and treatment time. The best photocatalytic performance was attained for the samples with needle-like morphology.

1. Introduction

Nowadays, the environmental problems demand increasingly severe regulations that open up opportunities for novel green photocatalytic routes leading to the alternative materials to traditional TiO_2, in order to allow the use of sunlight as the energy source for pollutant abatement [1]. For this scope the use of visible light photons constitutes the key point for a good photocatalyst performance under sunlight conditions. Among the family of new photocatalysts recently proposed, $BiVO_4$ ($E_g = 2.40$ eV) has been widely reported exhibiting good photocatalytic properties [2]. Bismuth vanadate ($BiVO_4$) has three main crystalline structures: zircon-tetragonal, scheelite-tetragonal and scheelite-monoclinic. $BiVO_4$ can be synthesized by different preparation routes which allow obtaining selectively one of the mentioned structures with different morphologies depending on the preparation method [3–7]. Regarding to scheelite-like compound, the monoclinic structure is usually obtained by means of high temperature methods. Meanwhile, the tetragonal form is normally achieved by aqueous media methods at low temperature process. However, from the literature data, it arises that the most photoactive phase is the monoclinic one. So, the attempts of achieving this crystalline phase are of great importance. The use of hydrothermal treatments for the preparation of $BiVO_4$ leads to the appearance of the monoclinic phase at mild temperatures with lower crystallite sizes with respect to those obtained from solid state reaction [8,9]. Thus, Zhang et al. proposed the synthesis of monoclinic $BiVO_4$ nanosheets by means of hydrothermal method assisted by a morphology-directing agent [5]. These nanosheet-shape material exhibits much higher photocatalytic activity for solar photodegradation of rhodamine B than the bulk material. In this sense, m-$BiVO_4$ structure with high surface area was also obtained by means of K_2SO_4 as inorganic shape-controlling additive. Recently, Xi and Ye reported a novel hydrothermal synthetic procedure to obtain m-$BiVO_4$ nanoplates showing preferential exposition of [0 0 1] facets [10]. Similarly to Bi_2MoO_6 systems, this preferentially exposed facet seems to produce an enhanced photoactivity for the degradation of organic contaminants as well as for the photocatalytic oxidation of water to O_2. By comparison the m-$BiVO_4$ nanorods with [1 0 0] growth direction, the nanoplates showed remarkably higher photoactivity in spite of its lower surface area with respect to the nanorods [11,12]. This clearly points out the fact that in this material the photoactivity is more related to the surface (or shape) structure than in the surface area. Moreover, Zheng et al. proposed a similar procedure using a Gemini surfactant and producing 3D hierarchical structure [13]. The influence of the particular morphology has been also pointed out by Zhou et al. [14]. They reported the preparation of monoclinic $BiVO_4$ microtubes particles forming flowerlike structures and exhibiting a prominent improvement in the photocatalytic activity. Such notably visible photoactivity seems to be attributed to the distinctive morphology. In spite of

* Corresponding author. Tel.: +34 954489536.
E-mail address: gcolon@icmse.csic.es (G. Colón).

0926-3373/$ – see front matter © 2011 Elsevier B.V. All rights reserved.
doi:10.1016/j.apcatb.2011.12.037

the strong influence of morphological aspects, high surface area system is still needed in order to achieve a high photoactive material [15].

In the present paper, we report a simple surfactant free hydrothermal method which allows obtaining $BiVO_4$ monoclinic systems with controlled morphology. The relationship between surface area, structure and morphology with the further photocatalytic activity for methylene blue degradation has been also performed.

2. Experimental

2.1. Synthesis of photocatalysts

The preparation of $BiVO_4$ was carried out by mixing the corresponding amounts of $Bi(NO_3)_3{\cdot}5H_2O$ and NH_4VO_3. Thus, 5 mmol of the Bi precursor was dissolved in 10 ml of glacial acetic acid while the stoichiometric amount of NH_4VO_3 (5 mmol) was dissolved in 60 ml of bidistilled water. These two solutions were finally mixed to form a yellowish suspension (pH 1 approx.) which is kept under stirring for 1 h. Similar series were prepared but in this case after the precipitation the pH was settled at 5 and 9 by adding NH_4OH or triethylamine (TEA) as pH controlling agent. Then, the resulting suspension was transferred into a Teflon recipient inside of stainless steel autoclave. The hydrothermal treatment was performed at 100 °C or 140 °C for different times between 2 and 20 h. The precipitate was then filtered, repeatedly washed and dried overnight at 120 °C. Afterwards, thus obtained samples were submitted to a further calcination treatment at 300 °C for 2 h. Samples were named as N or T depending on the precipitating agent (ammonia or TEA), followed by the pH value, hydrothermal temperature and time (i.e. N5-100-2 h refers to the sample precipitated with NH_4OH at pH 5 and hydrothermally treated at 100 °C for 2 h).

2.2. Materials characterization

BET surface area and porosity measurements were carried out by N_2 adsorption at 77 K using a Micromeritics 2010 instrument.

X-ray diffraction (XRD) patterns were obtained using a Siemens D-501 diffractometer with Ni filter and graphite monochromator. The X-ray source was Cu Kα radiation (0.15406 nm). Crystallite sizes and lattice strain parameters for $BiVO_4$ catalysts were estimated from the line broadening of (1 2 1) X-ray diffraction peaks by using the XPert HighScore Plus software.

The morphology of samples was followed by means of field emission-SEM (Hitachi S 4800). The samples were dispersed in ethanol using an ultrasonicator and dropped on a copper grid.

UV–vis spectra were recorded by using a Shimadzu AV2101 in the diffuse reflectance mode (R) and transformed to a magnitude proportional to the extinction coefficient (K) through the Kubelka–Munk function, $F(R_\infty)$. Samples were mixed with $BaSO_4$ that does not absorb in the UV–vis radiation range (white standard). Scans range was 250–800 nm.

2.3. Photocatalytic experimental details

The methylene blue (MB) oxidation reactions were performed using a batch reactor (150 ml) using a low power Xenon lamp. The intensity of the incident UVA light on the solution was measured with a PMA 2200 UVA photometer (Solar Light Co.) being ca. 10 W/m^2 (UVA PMA2110 sensor; spectral response 320–400 nm). On the other hand, the intensity of light in the visible range measured in this case is 35 W/m^2 (Photopic PMA21300 sensor; spectral response 400–700 nm). In the oxidation tests, an oxygen flow was employed what produces a homogenous suspension of the catalyst in the solution. Before each experiment, the catalysts (1 g/L) were settled in suspension with the reagent mixture for 15 min, after which an adsorption rate of MB below 3% is observed in all cases. The blank experiment was run without catalyst and no MB degradation was observed after 2 h. The evolution of the initial MB concentration (ca. 10 ppm) was followed through the evolution of the characteristic 664 nm band using a centrifuged aliquot ca. 2 ml of the suspension (microcentrifuge Minispin, Eppendorf).

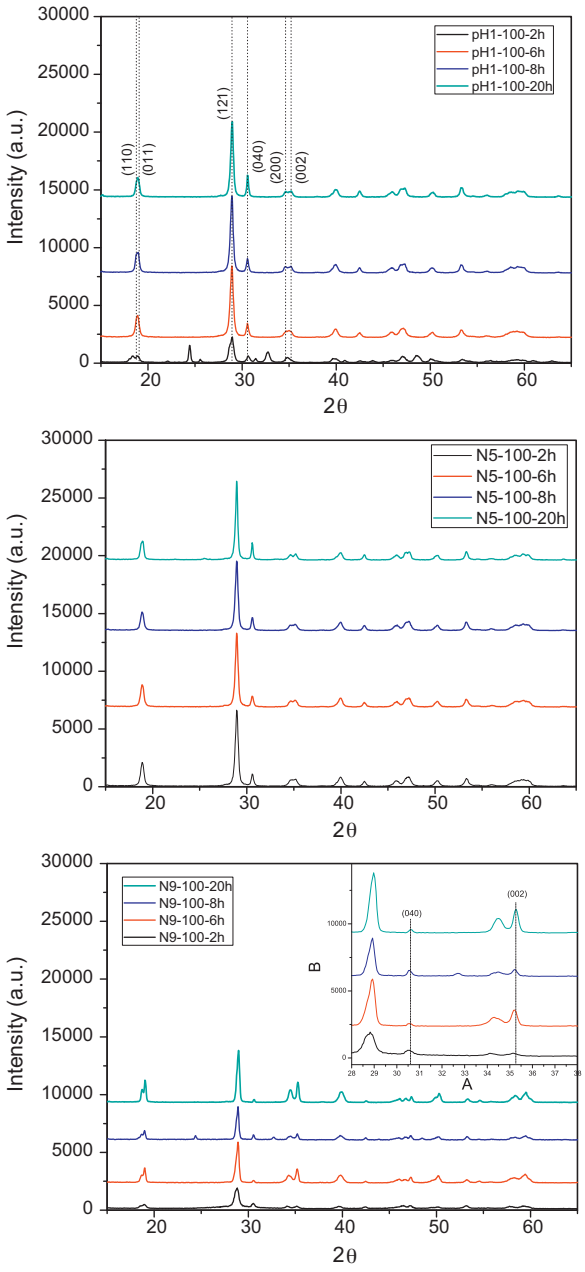

Fig. 1. XRD patterns for $BiVO_4$ samples prepared by hydrothermal treatment at 100 °C using NH_4OH as pH controlling agent.

3. Results and discussion

3.1. Hydrothermal synthesis of $BiVO_4$ with ammonia

The preparation at low pH value leads to well crystallized scheelite $BiVO_4$ structure in the monoclinic phase (*JCPDS 14-0688*, corresponding to the *I*2/*a* space group). However, at the initial state of the hydrothermal treatment at 100 °C a mixture of

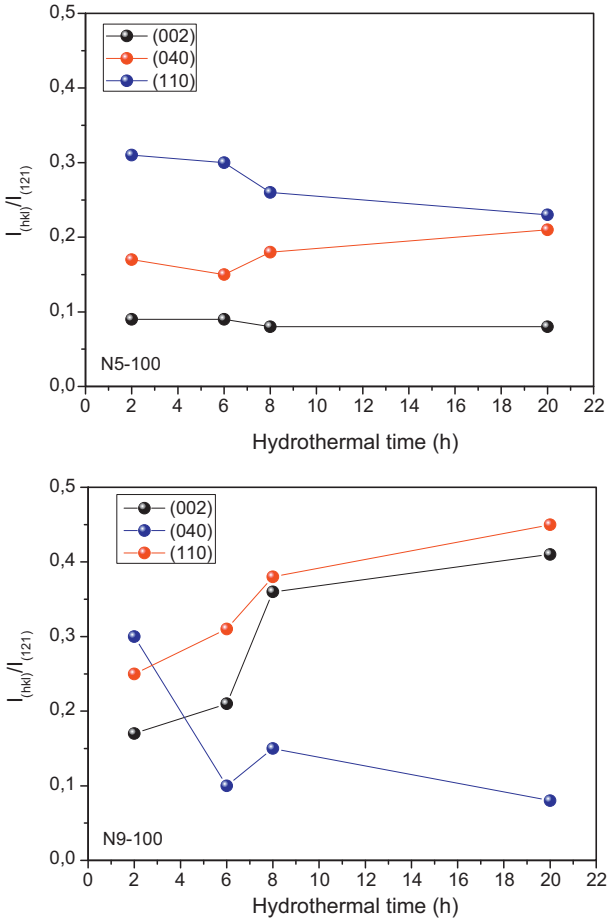

Fig. 2. Evolution of the relative intensity for (0 0 2), (0 4 0) and (1 1 0) planes for $BiVO_4$ samples prepared by hydrothermal treatment at 100 °C using NH_4OH (a) at pH 5 and (b) at pH 9.

tetragonal and monoclinic phase can be observed (Fig. 1). In the same direction, samples prepared by hydrothermal method using NH_4OH (at pH 5 and pH 9) presented only the monoclinic phase. It is worthy to note that the preparation with NH_4OH at pH 9 leads to an interesting structural evolution with the hydrothermal time. By observing the relative intensities of the diffraction peaks, a clear preferential orientation is present. Thus, the relative intensity of the diffraction line for (0 4 0) appears notably diminished, at the same time the diffraction peaks corresponding to (1 1 0) and (0 0 2) planes notably rise up as hydrothermal time increases (Fig. 2). This preferential orientation was not observed in the series obtained at lower pH values and would denote a change in the morphology. In Table 1 we summarize the crystallite size and lattice strain for this series. For all the series, the crystallite size progressively increases as hydrothermal time increases, varying from 29 to 37 nm. At the same time, the lattice strain decreases with the hydrothermal time, indicating that upon hydrothermal treatment the crystallinity of samples increases. In the case of N5-100 series, the sample obtained after 20 h of hydrothermal treatment exhibits a significantly higher crystallite size.

Regarding the BET surface area, all catalysts present low values which vary depending on the preparation series (Table 1). This fact is a common feature of $BiVO_4$ reported in the literature. In order to overcome this problem, some authors use the aid of surfactant to increase the surface area values [16]. In our case, the obtained values are slightly higher with respect most of the reported one without employing surfactant. The general evolution BET surface area for all series is similar, following a diminution with hydrothermal time. It is worthy to point out that for N5-100 series BET surface areas present slightly higher values with respect to the other series, being the diminution more significant with hydrothermal time. For the other series, the hydrothermal time does not affect to the surface area values, and in all cases S_{BET} lies around 2.5–3 m^2/g. A particular exception can be made for N9-100-2 h for which a remarked value is obtained.

The band gap values calculated from the diffuse reflectance spectra for all series were estimated to be between 2.3 and 2.4 (Table 1), which is consistent with the band gap for the monoclinic $BiVO_4$.

The morphology of $BiVO_4$ systems is notably affected by the pH of the precipitation (Fig. 3). At lower pH the $BiVO_4$ initially exhibits a hierarchical structure even at low hydrothermal time (Fig. 3a–c). The initial structure suffers an important evolution with time, forming at the end of the hydrothermal treatment a two assembled ball structure. As pH increases, the morphology changes drastically. Thus, at pH 5 peanut-like aggregates of 3–4 μm formed by rounded particles are observed (Fig. 3d–f). At large hydrothermal times, the peanut-like shape seems to collapse forming a similar ball assembled structure observed for samples prepared in the absence of ammonia. Recently, Shang et al. reported a similar 3D assembly obtained by surfactant-free hydrothermal synthesis [17]. These authors employed ethylene glycol to produce a Bi^{3+} complex which seems to favor the crystal splitting process [18]. Finally, at higher pH, the morphology develops from homogeneous rounded particles towards needle-like one (Fig. 3g–i). The differences observed in the morphology can be correlated with the evolution in the XRD pattern already discussed. Thus, for the samples prepared at pH 9 the preferential orientation observed for (1 1 0) and (0 0 2) planes is clearly associated with the needle like morphology (Fig. 4). The crystalline growth along the *b* axis to form the acicular particles leads to the extinction of the (0 4 0) diffraction line and the notably

Table 1
Surface, structural and photocatalytic characterization for $BiVO_4$ samples prepared by hydrothermal treatment at 100 °C using NH_4OH as pH controlling agent.

Sample	Crystallite size (nm)	Lattice strain (%)	Band gap (eV)	BET (m^2/g)	k ($\times 10^{-5}$ s^{-1})
pH1-100-2 h	29	0.609	2.32	3.0	3.7
pH1-100-6 h	28	0.624	2.31	3.0	5.5
pH1-100-8 h	33	0.551	2.32	2.8	6.2
pH1-100-20 h	37	0.502	2.27	2.7	7.3
N5-100-2 h	32	0.569	2.35	7.7	11.7
N5-100-6 h	33	0.548	2.35	5.4	7.3
N5-100-8 h	34	0.543	2.34	4.4	10.7
N5-100-20 h	49	0.410	2.39	3.3	5.0
N9-100-2 h	17	0.951	2.40	30.2	10.5
N9-100-6 h	31	0.583	2.41	2.0	2.8
N9-100-8 h	37	0.510	2.42	2.7	9.1
N9-100-20 h	37	0.502	2.38	1.6	8.8

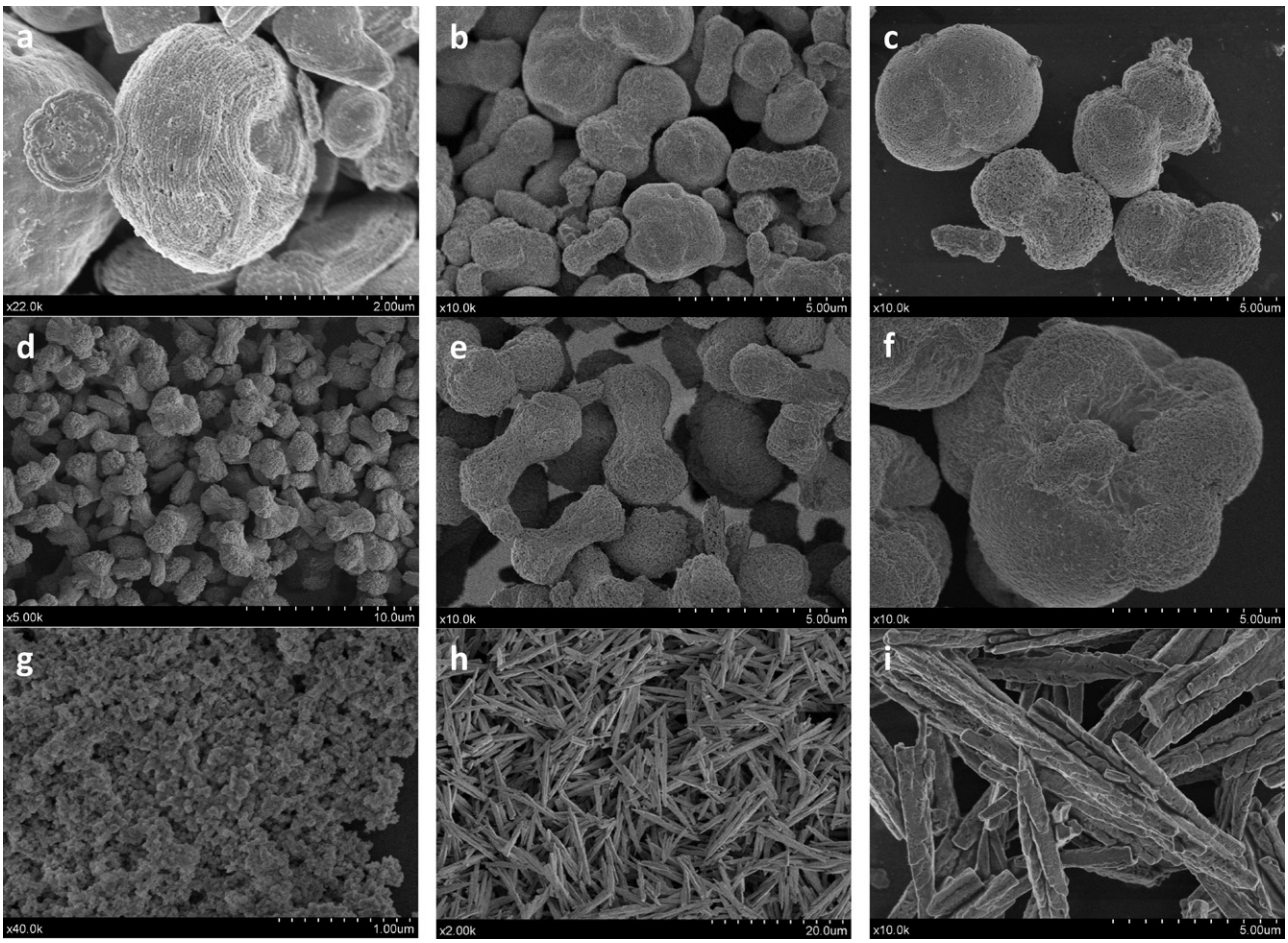

Fig. 3. SEM images of $BiVO_4$ samples prepared by hydrothermal treatment at 100 °C using NH_4OH. pH 1: (a) N1-100-2 h, (b) N1-100-6 h and (c) N1-100-20 h; pH 5: (d) N5-100-2 h, (e) N5-100-6 h and (f) N5-100-20 h; pH 9: (g) N9-100-2 h, (h) N9-100-6 h and (i) N9-100-20 h.

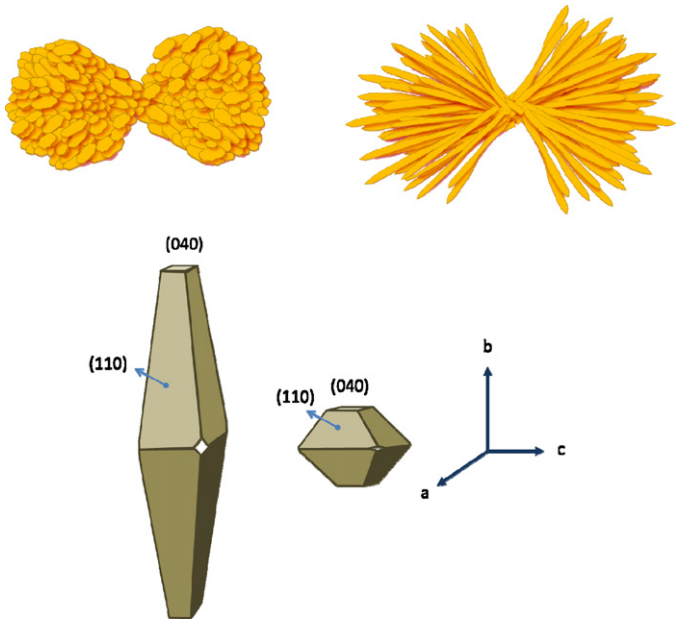

Fig. 4. Schematic illustration of different morphologies of $BiVO_4$.

exaltation of diffraction lines corresponding to the planes (1 1 0) and (0 0 2). From these results it is worthy to note that we could tune the morphology of the assembly, from peanut-like to needle-like architectures by changing the pH value and without using any surfactant additive.

The photocatalytic performance of the as-prepared m-$BiVO_4$ was evaluated by following the photodegradation of MB under UV–vis light irradiation (Fig. 5). From these results, it appears that all series present degradation rates directly affected by the hydrothermal time. In all cases, the best degradation rate is close to 50–60% after 2 h of irradiation, being a remarked value if we take into account the low power of the lamp. The reaction rates calculated for all series are depicted in Fig. 6. For samples prepared at pH 1, the reaction rate progressively increases with the hydrothermal time. This evolution could by related in principal with the increasing of the crystallinity since the surface area values for this series do not change during hydrothermal treatment. As above mentioned, the crystallite size and lattice strain increases and diminishes, respectively, as hydrothermal time progresses. The slight diminution of surface area seems to have no clear effect on the final photocatalytic performance. If we observe the evolution of the reaction rate for the series prepared at pH values of 5 and 9, in both cases, the initial trend is the opposite with respect to early series and the reaction rates diminish as hydrothermal time increases. However, though for N5-100 series the decrease is progressive, for N9-100 this tendency changes after 6 h of hydrothermal

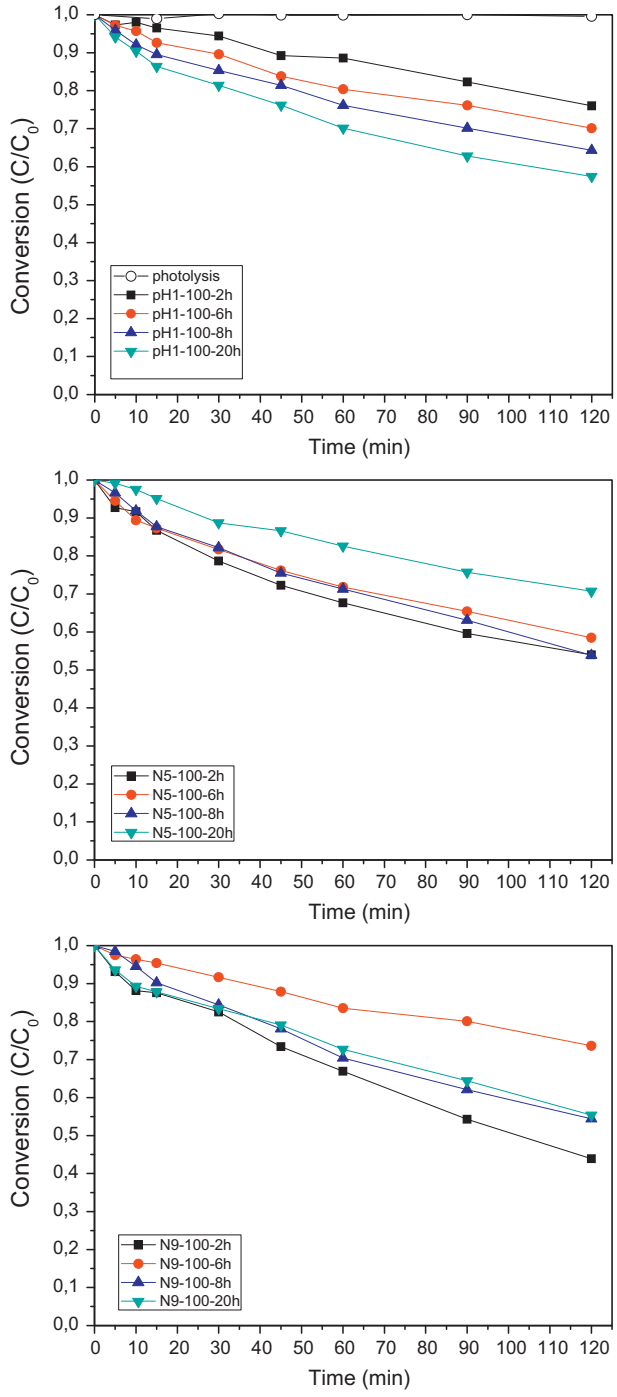

Fig. 5. Evolution of MB during photodegradation for $BiVO_4$ samples prepared by hydrothermal treatment at 100 °C using NH_4OH as pH controlling agent.

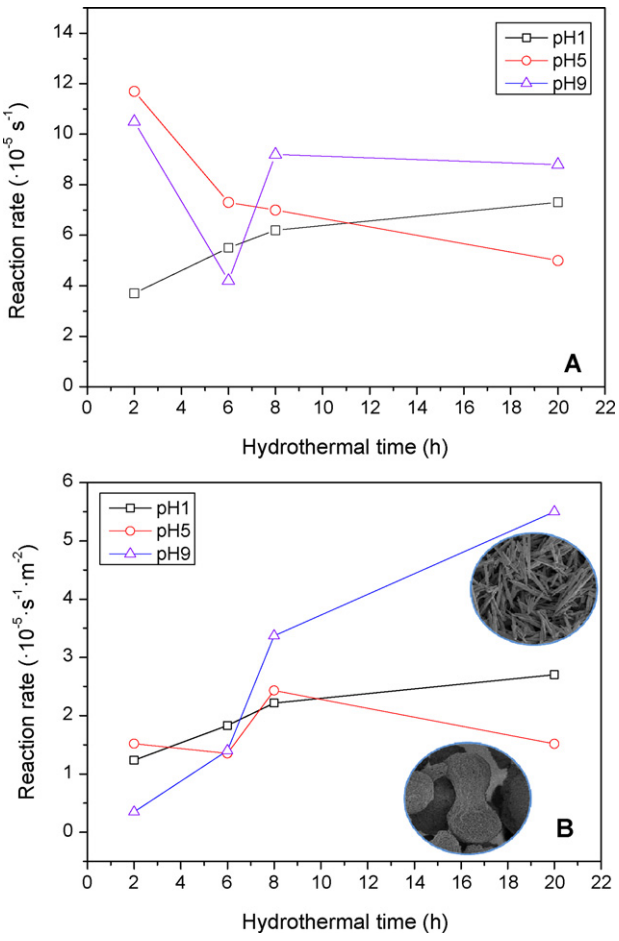

Fig. 6. (a) MB photodegradation reaction rates and (b) MB photodegradation specific reaction rates per surface area unit, for $BiVO_4$ samples prepared by hydrothermal treatment at 100 °C using NH_4OH as pH controlling agent.

treatment (Fig. 6a). Taking into account the evolution of the surface area, structure and morphology above discussed, the modification in the activity evolution could be associated with the appearance of the acicular shape in the particles. In order to evaluate the influence of surface area on the photocatalytic performance, we have represented the specific reaction rate by surface area unit (Fig. 6b). For the N5-100 series, the crystallite size values are almost constant meanwhile the surface area progressively decreases with hydrothermal time. So it can be assumed that this later parameter would directly affect to the photocatalytic activity evolution. In fact, the specific reaction rate for this series appears almost constant. In the case of N9-100 series, both the crystallite size and surface area do not change considerably along the hydrothermal time, so the inversion in the photoactivity tendency would be attributed to the particular morphology of the samples. For these samples a clear improvement in the specific reaction rate is observed which could be linked with the appearance of the needle-like particles.

3.2. *Effect of precipitating agent and hydrothermal temperature*

In order to have a deep insight on the effect of preparation parameter on the m-$BiVO_4$ structure and morphology, we have also study the effect of the precipitating agent and the temperature of the hydrothermal treatment. For this scope, we have used triethylamine (TEA) as pH controller. The use of TEA as precipitating agent has been previously described for the hydrothermal synthesis of Bi_2WO_6 and leading to controlled flowerlike hierarchical structures [19]. In Table 2 we summarize the surface and structural data for T5-100 series. As in the case of N series, $BiVO_4$ appears in the monoclinic structure, exhibiting no preferential orientation in the diffraction patterns (Fig. S1). The crystallite size progressively increases as hydrothermal time increases. From crystallite size and lattice strain values it can be inferred that the precipitation with TEA leads to a similar crystallinity situation with respect to N5-100 series. However, regarding to the surface area, it seems that in this case this parameter decrease slightly, presenting values around 4.5 m^2/g. Regarding to the optical properties, the band gap

Table 2
Surface, structural and photocatalytic characterization for $BiVO_4$ samples prepared by hydrothermal treatment at 100 °C using TEA as pH controlling agent.

Sample	Crystallite size (nm)	Lattice strain (%)	Band gap (eV)	BET (m^2/g)	k ($\times 10^{-5}$ s^{-1})
T5-100-2 h	34	0.539	2.35	4.7	12.3
T5-100-6 h	35	0.527	2.30	6.5	8.5
T5-100-8 h	42	0.454	2.38	4.2	6.8
T5-100-20 h	44	0.444	2.29	3.5	11.5

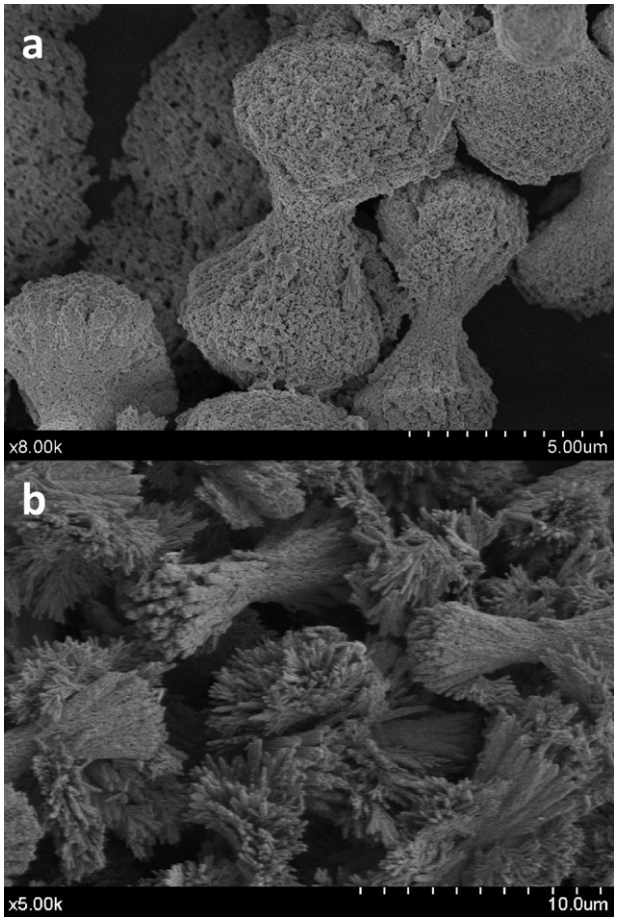

Fig. 7. SEM images of $BiVO_4$ samples prepared by hydrothermal treatment at 100 °C using TEA at pH 5. (a) T5-100-6 h and (b) T5-100-20 h.

values obtained are in all cases consistent with that associated to the monoclinic $BiVO_4$ structure.

Supplementary material related to this article found, in the online version, at doi:10.1016/j.apcatb.2011.12.037.

In Fig. 7 we show the SEM image for T5-100 after 6 and 20 h of hydrothermal treatment. The morphology for T5-100-6 h can be ascribed to peanut-like particles, which is similar to that observed for N5-100 (Fig. 3). However, after long hydrothermal

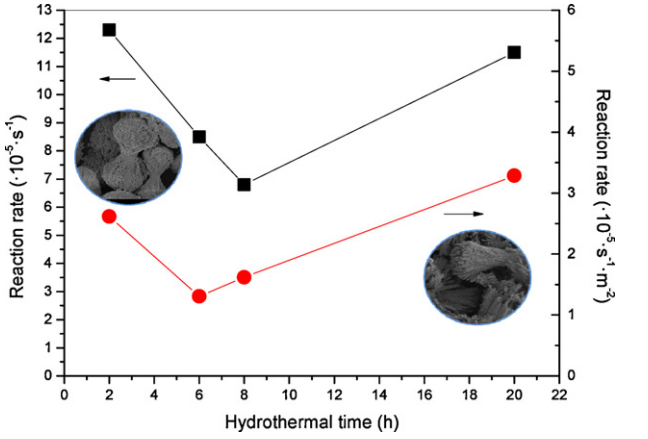

Fig. 8. MB photodegradation reaction rates for $BiVO_4$ samples prepared by hydrothermal treatment at 100 °C using TEA as pH controlling agent.

treatment the roundish assembly turns to acicular sheaf. This assembly is close to the previously reported morphology by Shang et al. [17]. We may induce that there exist an evolution of the rounded particles towards needle-like one, forming straw-sheaf structures.

Regarding the photoactivities for this T5-100 series, the conversion rates for MB degradation lie between 40 and 60% after 2 h of irradiation (Fig. S2). At low hydrothermal times, the calculated reaction rates for T5-100 follow a similar trend as for N5-100 series and decreases as hydrothermal time increases (Fig. 8). Then, the T5-100-20 h samples present higher reaction rate with respect to T5-100-20 h. This evolution is analogous to the progress of the N9-100 series. Again, the existence of acicular morphology in this sample would be related to the increase in the photoactivity. The specific reaction rate clearly follows the same trend, indicating that surface area value does not induce a significant effect. Therefore structural and morphological evolution of the sample (higher crystallinity and acicular morphology) is the responsible of the photocatalytic improvement. Comparing the progress of the reaction rates for this series with that observed for N5-100 one, it is clear that reaction rates presented for T5-100-20 h sample are better than the values observed for series obtained by precipitation with ammonia. This better performance is associated with the different morphology obtained in this case.

Table 3
Surface, structural and photocatalytic characterization for $BiVO_4$ samples prepared by hydrothermal treatment at 140 °C using NH_4OH and TEA as pH controlling agent.

Sample	Crystallite size (nm)	Lattice strain (%)	Band gap (eV)	BET (m^2/g)	k ($\times 10^{-5}$ s^{-1})
N5-140-2 h	35	0.530	2.32	3.6	7.7
N5-140-6 h	36	0.514	2.34	4.8	8.0
N5-140-8 h	39	0.488	2.31	3.3	6.3
N5-140-20 h	39	0.462	2.38	3.6	7.2
T5-140-2 h	34	0.532	2.36	8.0	9.8
T5-140-6 h	39	0.481	2.37	2.7	9.2
T5-140-8 h	43	0.449	2.33	2.7	8.8
T5-140-20 h	49	0.406	2.35	1.3	4.5

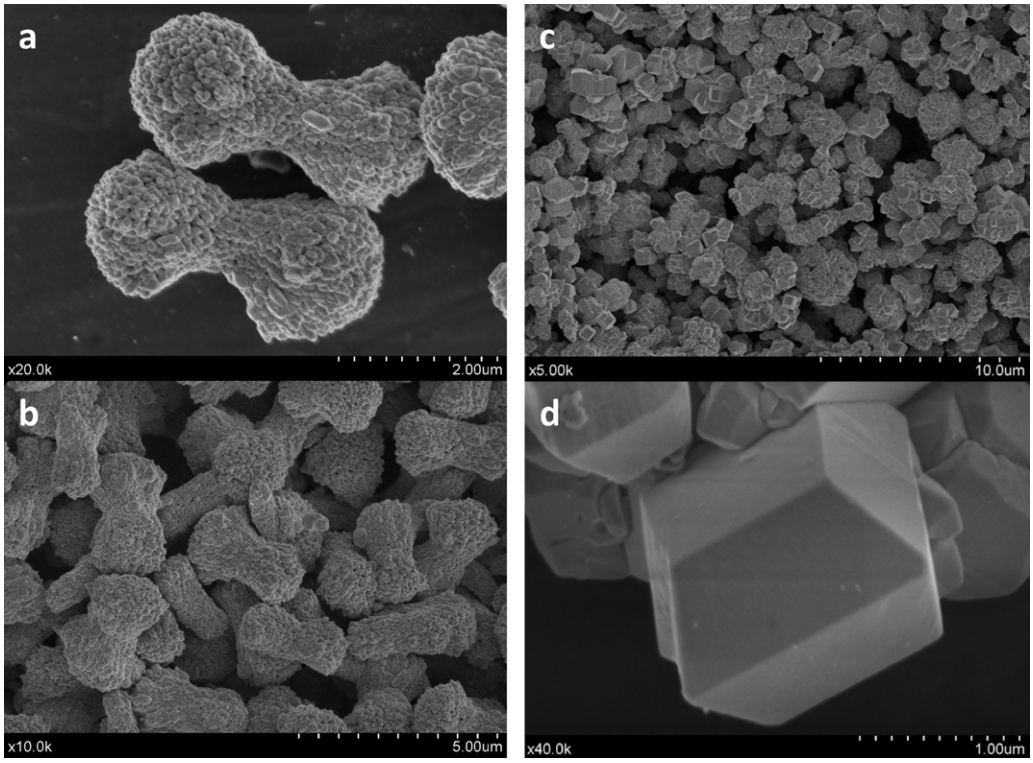

Fig. 9. SEM images of $BiVO_4$ samples prepared by hydrothermal treatment at 140 °C at pH 5 by means of NH_4OH (a) N5-140-6 h and (b) N5-140-20 h. And TEA, (c) T5-140-6 h and (d) T5-140-20 h.

Supplementary material related to this article found, in the online version, at doi:10.1016/j.apcatb.2011.12.037.

Following with the analysis of the factors influencing the structural and morphological features of $BiVO_4$, we increased the temperature of the hydrothermal treatment. In Table 3 we report the surface area and structural data for N5-140 and T5-140 series, prepared by using ammonia and TEA respectively. By examining the structural features, the monoclinic crystalline phase is the one present in both series (Fig. S3). As expected, the crystallite size increases as hydrothermal time increases. Furthermore, the growth the crystallite size is more markedly in T5-140 series. The evolution of surface area values is also different in both series. Thus, while for N5-140 the surface area values are found between 3 and 4 m^2/g, for T5-140 series the surface area notably decrease from 8.0 m^2/g to 1.3 m^2/g.

Supplementary material related to this article found, in the online version, at doi:10.1016/j.apcatb.2011.12.037.

It is noteworthy the differences in the morphology for these series (Fig. 9). Thus, N5-140 samples exhibit a peanut-like shape of 3–4 μm length, similar to the previous N5-100 samples. This 3D assembly is formed by roundish particles of about 200 nm. On the other hand, T5-140 series present a well-defined polyhedral shape that upon hydrothermal time appears as truncated octahedron. Therefore, it can be said that TEA may act as morphology directing agent. While the hydrothermal treatment at 100 °C leads to needle-like shaped particles, at higher temperature the morphology drastically changes to truncated octahedral-like particles with smoothed surfaces. This compact structure would lead to lower surface area.

The photocatalytic activity for N5-140 and T5-140 is also directly affected by the structural and morphological features of the samples, especially for T5-140 series (Fig. 10). In this sense, N5-140 systems exhibits similar reaction rates along the different hydrothermal times with conversion rates between 40% and 50% (Fig. S4). The T5-140 series shows a clear decreasing evolution in the photoactivity as hydrothermal treatment progresses, reaching a 30% conversion for the T5-140-20 h catalyst.

Supplementary material related to this article found, in the online version, at doi:10.1016/j.apcatb.2011.12.037.

This result can be related to those previously reported by Li's group in which a clear evolution from octahedral shape to plate-like morphology was found [11]. In that case, the excellent performance for O_2 evolution was related to the preferential exposition of (0 4 0) facets in the plate-like particles. These authors associated the exaltation of the photoactivity the fact that (0 4 0) facets provide multiatomic BiV_4 center, which would be the origin of the active sites for O_2 evolution reaction. Similar explanation was already given by Sun et al. for starlike $BiVO_4$ particles [11]. In that case the formation of this flat morphology was favored by the slower growth along the [0 1 0] direction which lead to the formation of the nanoplates along the (0 1 0) plane.

In our case, the best photocatalytic degradation rate for MB degradation reaction was attained by T5-100-20 h which presents a crystal splitting of 3D straw-sheaf architecture. The acicular morphology seems to provide better photocatalytic results in N9-100 and T5-100 series. For this morphology, only in the case of isolated needle-like particles the preferential orientation for (1 1 0) and (0 0 2) is observed in the diffraction pattern. The crystal splitting process for T5-100 leads to 3D hierarchical aggregation of the structure, avoiding this preferential exposition of (1 1 0) and (0 0 2) facets. On the contrary, well-defined polyhedral structure gives the worst photocatalytic results, probably due to the low surface area of the compacted polyhedral structures. Indeed, the specific reaction rates clearly indicate that compacted octahedra exhibit notably higher values indicating a strong influence with surface area.

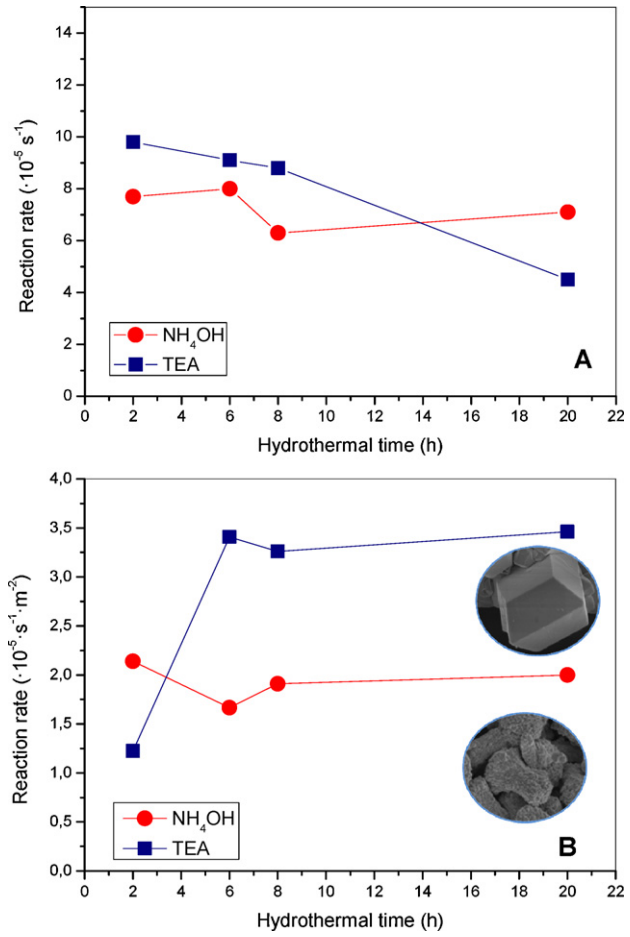

Fig. 10. (A) MB photodegradation reaction rates and (B) MB photodegradation specific degradation rates per surface area unit, for $BiVO_4$ samples prepared by hydrothermal treatment at 140 °C at pH 5 using NH_4OH and TEA as pH controlling agent.

4. Conclusions

We have obtained well crystallized m-$BiVO_4$ by a simple surfactant free hydrothermal method. By changing the pH, directing agent and hydrothermal parameters such as temperature and time, different morphologies have been obtained.

The best performance was clearly not associated to the surface area values, and is strongly affected by the crystallite size and morphology. For the different series obtained, better photocatalytic performances have been achieved for m-$BiVO_4$ with needle-like morphology. It is worthy to note that upon illumination with a low intensity lamp (35 W), the conversion rate for such system is about 60% degradation after 2 h of irradiation.

Acknowledgments

The financial support by the project P09-FQM-4570 is fully acknowledged. S. Obregón Alfaro thanks CSIC for the concession of a JAE-Pre grant.

References

[1] G. Colón, C. Belver, M. Fernández-García, Nanostructured oxides in photocatalysis, in: M. Fernández-García, J.A. Rodríguez (Eds.), Synthesis, Properties and Application of Oxide Nanoparticles, Wiley, USA, 2007, ISBN 978-0-471-72405-6 (Chapter 17).
[2] A. Kubacka, M. Fernández-García, G. Colón, Chem. Rev. (2011), doi:10.1021/cr100454n.
[3] S. Tokunaga, H. Kato, A. Kudo, Chem. Mater. 13 (2001) 4624.
[4] L. Zhang, D. Chen, X. Jiao, J. Phys. Chem. B 110 (2006) 2668.
[5] X. Zhang, Z. Ai, F. Jia, L. Zhang, X. Fan, Z. Zou, Mater. Chem. Phys. 103 (2007) 162.
[6] Y. Zhao, Y. Xie, X. Zhu, S. Yan, S. Wang, Chem. Eur. J. 14 (2008) 1601.
[7] L. Zhou, W. Wang, H. Xu, Cryst. Growth Des. 8 (2008) 728.
[8] L. Zhou, W. Wang, S. Liu, L. Zhang, H. Xu, W. Zhu, J. Mol. Catal. A: Chem. 252 (2006) 120.
[9] Y. Guo, X. Yang, F. Ma, X. Li, L. Xu, X. Yuan, Y.H. Guo, Appl. Surf. Sci. 256 (2010) 2215.
[10] G. Xi, J. Ye, Chem. Commun. 46 (2010) 1893.
[11] S. Sun, W. Wang, L. Zhou, H. Xu, Ind. Eng. Chem. Res. 48 (2009) 1735–1739.
[12] D. Wang, H. Jiang, X. Zong, Q. Xu, Y. Ma, G. Li, C. Li, Chem. Eur. J. 17 (2011) 1275–1282.
[13] Y. Zheng, J. Wu, F. Duan, Y. Xie, Chem. Lett. 36 (2007) 520.
[14] L. Zhou, W. Wang, L. Zhang, H. Xu, W. Zhu, J. Phys. Chem. C 111 (2007) 13659.
[15] G. Li, D. Zhang, J.C. Yu, Chem. Mater. 20 (2008) 3983–3992.
[16] H. Jiang, H. Dai, X. Meng, K. Ji, L. Zhang, J. Deng, Appl. Catal. B: Environ. 105 (2011) 326–334.
[17] M. Shang, W. Wang, J. Ren, S. Sun, L. Zhang, CrystEngComm 12 (2010) 1754–1758.
[18] J. Tang, A.P. Alivisatos, Nano Lett. 6 (2006) 2701–2706.
[19] G. Colón, S. Murcia López, M.C. Hidalgo, J.A. Navío, Chem. Commun. 46 (2010) 4809–4811.